Pharm Res (2014) 31:3289–3303
DOI 10.1007/s11095-014-1418-z

RESEARCH PAPER

Folate and TAT Peptide Co-Modified Liposomes Exhibit Receptor-Dependent Highly Efficient Intracellular Transport of Payload In Vitro and In Vivo

Yaqin Zhu • Liang Cheng • Lifang Cheng • Fazhen Huang • Qing Hu • Ling Li • Chenmin Tian • Lin Wei • Dawei Chen

Received: 11 February 2014 / Accepted: 12 May 2014 / Published online: 24 May 2014

ABSTRACT

Purpose Using different chain lengths of PEG as linkers to develop a novel folate (FA) and TAT peptide co-modified doxorubicin (DOX)-loaded liposome (FA/TAT-LP-DOX) and evaluate its potential for tumor targeted intracellular drug delivery.

Methods FA/TAT-LP-DOX was prepared by pH gradient method and post-insertion method and the optimal ligand density was screened by MTT assay. *In vitro* evaluation was systematically performed through cytotoxicity assay, cellular uptake studies, subcellular localization and cellular uptake mechanism in folate receptor (FR) over-expressing KB tumor cells. *In vivo* tumor targeted delivery of FA/TAT-LP-DOX was also studied by *in vivo* fluorescence imaging in a murine KB xenograft model.

Results The particle size and zeta potential determination indicated that FA and TAT were successfully inserted into the liposome and cationic TAT peptide was completely shielded. With the optimal ligand density (5% of FA and 2.5% TAT), the FA/TAT-LP-DOX exhibited improved cytotoxity and cellular uptake efficiency compared with its single-ligand counterparts (FA-LP-DOX and PEG/TAT-LP-DOX). Competitive inhibition and uptake mechanism experiments revealed that FA and TAT peptide played a synergistic effect in facilitating intracellular transport of the liposome, and association between FA and FA receptors activated this transport process. *In vivo* imaging further demonstrated the superiority of FA/TAT-LP in tumor targeting and accumulation.

Conclusions Folate and TAT peptide co-modified liposome using different chain lengths of PEG as linkers may provide a useful strategy for specific and efficient intracellular drug delivery.

KEY WORDS cellular uptake · folate · liposomes · TAT peptide · tumor targeted delivery

ABBREVIATIONS

CLSM	Confocal laser scanning microscopy
CME	Clathrin-mediated endocytosis
DCC	Dicyclohexylcarbodiimide
DLS	Dynamic laser scattering
DMEM	Dulbecco's modified Eagle's medium
DOX	Doxorubicin
DSPE	Distearoyl phosphatidylethanolamine
DSS	Disuccinimidyl suberate
EPR	Enhanced permeability and retention
FA	Folate
FR	Folate receptor
IFP	Interstitial fluid pressure
LP	Liposome
MTT	Thiazolyl blue tetrazolium bromide
NHS	N-hydroxysuccinimide
PLL	Polylysine
SPC	Soybean phospholipids
TAT	Trans-activating transcriptional activator
TEA	Triethylamine
TLC	Thin layer chromatography

INTRODUCTION

Exploiting the enhanced permeability and retention (EPR) effect (1,2), nanocarriers 20–200 nm in size can passively accumulate at tumor sites (3). Further modifications of nanocarriers by hydrophilic flexible polymeric materials are potentially beneficial for the time-dependent passive accumulation due to protection of nanocarriers from fast clearance by the Reticulo-Endothelial System (3,4). The second-generation doxorubicin liposome (Doxil®) supports this notion, and has

Yaqin Zhu and Liang Cheng contributed equally to this work.

Y. Zhu • L. Cheng • L. Cheng • F. Huang • Q. Hu • L. Li • C. Tian • L. Wei • D. Chen (✉)
Department of Pharmaceutics, College of Pharmaceutical Sciences
Soochow University, 199 Ren'ai Road, Suzhou 215123, China
e-mail: chendawei@syphu.edu.cn

exhibited superior drug efficacy in clinical practice (5). However, enhancing cellular uptake of nanocarriers in tumors is still of great concern.

To our knowledge, the transvascular and interstitial transport of nanocarriers is mainly driven by convection and diffusion. By contrast, the elevated interstitial fluid pressure (IFP) in tumors impels the movement of interstitial fluid into surrounding tissues, thus hampering effective penetration of nanocarriers from the solid mass (6–8). The factors determined the transport of nanocarriers to tumors were illustrated in Fig. 1a. If nanocarriers extravasated through the fenestrations of leaky tumor vasculatures could be rapidly taken by tumor cells, the adverse effect caused by high IFP would be alleviated to a great extent (9). In view of this, ligand modification strategy has been widely adopted in the design of nanocarriers on the basis of the fact that surfaces of most tumor cells highly express some specific receptors (3,10). Attachment of targeting ligands to nanocarriers ensures selective cellular binding and enhanced cellular uptake *via* receptor-mediated endocytosis (3,4). However, it should be noted that in most case the used ligand does not effectively improve the efficiency of intracellular transport of nanocarriers, probably due to its lack of enough membrane penetrating ability in addition to that density of cell surface receptors is usually not constant and saturation phenomenon always occurs (11,12).

Trans-activating transcriptional activator peptide, *i.e.* TAT peptide, has received extensive attention for its capacity of translocating cell membranes and efficient intracellular delivery of various cargoes (13–15). Even if the definite mechanisms for TAT peptide across cell membrane are still unclear, many studies have suggested that positive charges of TAT peptide play a key role in the uptake process (14,16,17). However, TAT peptide is a non-specific ligand, which limits its applications especially in targeted drug delivery (18). To overcome this deficiency, two major approaches have recently emerged. One approach was to attach TAT peptide to the distal end of short chain PEG and shield it through cleavable long chain PEG using disulfide or hydrazone bond as linkers (19,20). In the other approach, TAT peptide was directly attached to the surface of nanocarrier, then shielded by non-cleavable PEG chain whose hydrophilic end was further decorated with specific ligand (21). Remarkably, there is a common ground underlying the two approaches: TAT peptide is expected to exert its transmembrane ability upon nanocarriers arriving at tumor sites.

Enlightened by aforementioned work, we assume that simultaneous attachment of TAT peptide and specific ligand to nanocarrier using different molecular weights of PEG as linkers may take advantage of the respective merits of non-specific and specific ligands. In our case, liposome was selected as the model nanocarrier because of its ease to prepare as well as that ligand densities on liposomal surface were easily adjusted by post-insertion method (22). Folate (FA) was selected as the specific ligand since folate-mediated targeting has been demonstrated effective both *in vitro* and *in vivo* (23–25). FA was attached to the liposome using long chain PEG (MW 5,000), while TAT peptide was attached to the liposome using short chain PEG (MW 2,000). Doxorubicin was chosen as the payload in that it could be loaded into liposome with high entrapment efficiency by a pH-gradient method and used as a fluorescence probe. KB cell line, which overexpresses folate receptors, was used as the tumor cell model.

Schematic illustration of this dual-ligand nanocarrier was showed in Fig. 1b. The potential advantages of such a nanocarrier are that: (i) Specific ligand conjugated to the distal end of long chain PEG allows full exposure to cell surface receptors and favors tumor recognition and following receptor-mediated endocytosis. Additionally, long chain PEG is able to protect TAT peptide from opsonization during blood circulation. (ii) Application of flexible short chain PEG to anchor TAT peptide, not rigid coupling to connect TAT peptide to nanocarrier, partly minimize steric hindrance effect of long chain PEG on TAT peptide and is beneficial to free interaction of TAT peptide with the plasma membrane (26). (iii) PEG offers a wide variety of functional groups, making chemical conjugation of ligands to the nanocarrier convenient and controllable (27,28). (iv) Moreover, efficient intracellular transport of the dual-ligand liposome is highly dependent on the receptors overexpressed on the surfaces of tumor cells, unlike the stimuli-cleavable nanocarriers, there is no need for any additional manual operation.

In this study, FA/TAT-LP-DOX was first constructed with screened optimal density of each individual ligand. *In vitro* cytotoxicity and cellular uptake studies were conducted to ascertain whether this liposomal nanocarrier could achieve synergistic antitumor activity and enhanced cellular uptake efficiency. A further point of interest of this study was to elucidate the potential cellular entry mechanisms of the nanocarrier, which would make us better understand the exact role of FA and TAT peptide in cellular uptake of the nanocarrier. Finally, animal model of tumor-bearing mice was built, and *in vivo* tumor targeted delivery of the nanocarrier over time was monitored by near-infrared imaging system.

MATERIALS AND METHODS

Materials

Distearoyl phosphatidylethanolamine (DSPE) was purchased from Advanced Vehicle Technology Co., Ltd (Shanghai,

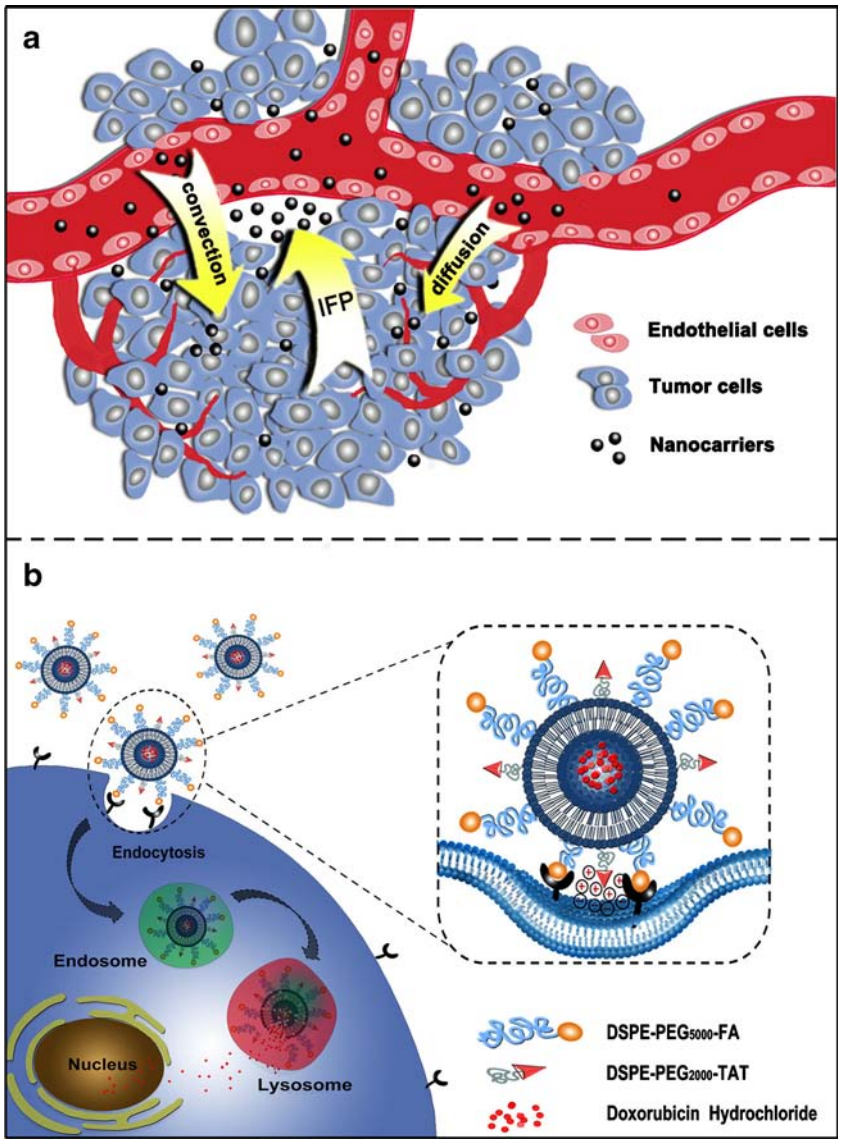

Fig. 1 Schematic illustration of impetus and resistance for transvascular and interstitial transport of nanocarriers (**a**) and the dual-ligand modification strategy achieving superior tumor-specific penetration (**b**).

China); Soybean phospholipids (SPC) were purchased from Tywei pharmaceuticals (Shanghai, China); Cholesterol and folate (FA) were obtained from sinopharm chemical reagent Co., Ltd (Shanghai, China); Dicyclohexylcarbodiimide (DCC), disuccinimidyl suberate (DSS) and N-hydroxysuccinimide (NHS) were purchased from Sigma (St Louis, MO, USA); DSPE-PEG_{2000}-Mal, $mPEG_{5000}$-DSPE and $mPEG_{2000}$-DSPE were purchased from Avanti Polar Lipids Inc (Alabaster, AL, USA); H_2N-PEG_{5000}-NH_2 were from Yarebio (Shanghai, China); TAT peptide with terminal Cysteine (Cys-AYGRKKRRQRRR) was synthesized by GL Biochem Co., Ltd. (Shanghai, China); Doxorubicin Hydrochloride was from Hua Feng United Technology Co., Ltd (Beijing, China); Folate-free DMEM culture media and newborn calf serum were purchased from Every Green Organism Engineering Materials Co., Ltd (Hangzhou, China); Lysotracker Green was obtained from Molecular Probes (Eugene, OR, USA). Hoechst 33342, polylysine (PLL), chloropromazine and colchicine were all from Sigma (St Louis, MO, USA) and filipin III was from Cayman Chemical (Ann Arbor, MI). Cy7 mono NHS ester was from Mycomebio Biomedical Science and Technology Center (Beijing, China). All other chemicals and reagents used were of analytical purity grade or higher, obtained commercially.

Human oral epithelial carcinoma cell line (KB) was purchased from cell bank of Chinese Academy of Sciences (Shanghai, China). Female Balb/c nude mice of 4–6 weeks age were purchased from Shanghai SLAC laboratory animal Co., Ltd. (Shanghai, China). Mice were housed at 25°C and 55% of humidity under natural light/dark conditions and allowed free access to standard folate-free food and water (Shanghai SLAC laboratory animal Co., Ltd., Shanghai, China). All animal procedures were performed following protocol approved by the Animal Study Committee of Soochow University.

Synthesis of DSPE-PEG$_{5000}$-FA

DSPE-PEG$_{5000}$-FA was synthesized as described previously (29). First, FA-PEG$_{5000}$-NH$_2$ was synthesized by reacting 200 mg NH$_2$-PEG$_{5000}$-NH$_2$ with 11 mg folate in 5 ml DMSO containing 5 mg NHS, 10 mg DCC and 15 μl TEA. The reaction mixture was stirred overnight in the dark at room temperature. Then 5 ml water was added into the reaction mixture and the insoluble by-product, dicyclohexylurea (DCU), was removed by centrifugation (3,000 rpm, 5 min). The supernatant was then dialyzed against 5 mM $NaHCO_3$ buffer (pH 9.0) and then against deionized water to remove the DMSO and unreacted folate in the mixture. The solution was then lyophilized and analyzed by TLC and ^{1}H-NMR. Second, 10 mg DSPE dissolved in $CHCl_3$ was reacted with 6 mg DSS in the presence of 10 μl TEA overnight at room temperature to yield an activated lipid anchor, DSPE-CO-(CH$_2$)$_6$-CO-NHS. Finally, equimolar of FA-PEG$_{5000}$-NH$_2$ and DSPE-CO-(CH$_2$)$_6$-CO-NHS were reacted in $CHCl_3$ overnight at room temperature. The solvent was removed on a rotary evaporator and the product was suspended in 50 mM Na_2CO_3 water solution to form micelles and then dialyzed against deionized water using a membrane with molecular weight cut-off (MWCO) 8,000 ~ 14,000 Da. The product was then lyophilized and analyzed by TLC and ^{1}H-NMR.

Synthesis of DSPE-PEG$_{2000}$-TAT

DSPE-PEG$_{2000}$-TAT was synthesized as described previously (19). Briefly, 15 mg DSPE-PEG$_{2000}$-Mal and 12 mg Cys-TAT were reacted in 5 ml water with gentle stirring at room temperature for about 30 h. The reaction progress was monitored by TLC. The solvent was then dialyzed against deionized water using a membrane with MWCO 8,000 ~ 14,000 Da for 48 h. The product was then lyophilized for use. The conjugation efficiency of TAT to DSPE-PEG$_{2000}$-Mal was analyzed by HPLC. Promosil Column: C$_{18}$ (4.6 mm × 250 mm, 5 μm); Mobile phase: solution A, pure water and solution B, acetonitrile, both containing 0.1% trifluoroacetic acid; Gradient elute: 0 ~ 16 min, 12% ~ 37% B; Flow rate: 1.0 ml/min; Wavelength: 220 nm; injection volume: 20 μl.

Preparation of Liposomes

Liposomes were prepared by the thin film hydration method and doxorubicin hydrochloride was loaded by the pH gradient method. Firstly, SPC and Cholesterol (2:1 molar ratio) were dissolved in ethanol and dried on a rotary evaporation at 37°C under vacuum. The lipid film was then hydrated with pH 4.0 citric acid buffer. Then it was sonicated by probe sonicator (100 W, 400 s) and finally homogenized by high pressure microfluidization (Nano DeBEE, USA) at 20,000 psi for 300 s.

For *in vivo* imaging investigations, DSPE was decorated with Cy7 by reacting DSPE and near-infrared (NIR) fluorophore, Cy7-NHS, and then DSPE-Cy7 was incorporated into liposomes at about 0.5 mol% of total lipids.

To obtain doxorubicin loaded liposomes (LP-DOX), the external phase of liposomes was adjusted to pH 7.6 by phosphate buffer. Then doxorubicin, at a drug-to-lipid molar ratio of 1:15, was dissolved in it and incubated at 70°C for 30 min. Unencapsulated doxorubicin was removed by dialysis.

Targeted liposomes FA/TAT-LP-DOX were prepared by the post-insertion method (22). DSPE-PEG$_{5000}$-FA and DSPE-PEG$_{2000}$-TAT were rehydrated with water to form micelles and then mixed with doxorubicin liposomes at 55°C for 1 h to allow insertion. Following heating, liposomes were immediately cooled on ice. Other types of liposomes (mPEG$_{5000}$-LP-DOX、mPEG$_{2000}$-LP-DOX、FA-PEG$_{5000}$-LP-DOX and TAT-PEG$_{2000}$-LP-DOX, abbreviated as PEG-LP-DOX、PEG$_{2000}$-LP-DOX、FA-LP-DOX、TAT-LP-DOX, respectively) were prepared as the same method.

Characterization of Liposomes

The mean diameter and zeta potential of liposomes were determined by dynamic light scattering (DLS) using a Nicomp TM380 ZLS (NICOMP, USA). Morphological analysis of liposomes was carried out by transmission electron microscopy (TEM) (TecnaiG220, FEI, USA).

The entrapment efficiency of doxorubicin liposomes was determined by the ultra filtration-HPLC method. Briefly, 500 μl doxorubicin liposomes were added to ultrafiltration devices (Millipore UFC501096) and centrifuged at 10,000 rpm for 15 min. Then free doxorubicin was collected and its concentration was determined by HPLC. Promosil Column: C$_{18}$ (4.6 mm × 250 mm, 5 μm); Mobile phase: solution A (0.01 mol/L $NH_4H_2PO_4$ buffer solution) : solution B (methanol) = 35:65; Flow rate: 1.0 ml/min; Wavelength: 497 nm; injection volume: 20 μl.

Doxorubicin encapsulation efficiency (EE, %) was calculated as follows.

$$EE\% = (\text{weight of the feeding drug} - \text{weight of the unencapsulated drug}) / \text{weight of the feeding drug} \times 100\%$$

In Vitro Release of DOX

The release profiles of DOX from FA/TAT-LP-DOX were studied at 37°C using a dialysis tube (MWCO 12,000) under shaking (200 rpm) in three different media, *i.e.* phosphate

buffer pH 7.4, phosphate buffer pH 6.8 and acetate buffer pH 5.0. Typically, 0.5 ml FA/TAT-LP-DOX was dialyzed against 20 ml of release media. At desired time intervals, 5 ml release media was taken out and replenished with an equal volume of fresh media. The amount of released DOX was determined by using fluorescence (FLS920) measurement (Ex=480 nm, Em=560 nm). The release experiments were conducted in triplicate and data are expressed as means ± SD.

Cell Culture

KB Cells were maintained in folate-free DMEM medium supplemented with 1% penicillin, 1% streptomycin, and 10% newborn calf serum. The cells were cultured as a monolayer in a humidified atmosphere containing 5% CO_2 at 37°C.

In Vitro Cytotoxicity Assay

Cytotoxicity studies were conducted by seeding KB cells at a density of 5×10^3 cells/well of a 96-well plate 24 h prior to incubation with liposomes. The culture medium was then replaced with 100 μl of medium containing different types of doxorubicin liposomes at different DOX concentrations. Following 72 h incubation at 37°C, the cells were washed with PBS and then 20 μl MTT stock solution (5 mg/ml) was added to each well, and the plates were further incubated for 4 h at 37°C in the dark. Medium was then discarded and 100 μl DMSO was added to dissolve the blue formazan crystal. Cell viability was assessed by absorbance at 492 nm measured on a microplate reader (Multiskan MK3, Thermo Labsystems, Finland). The data were expressed as the percentages of viable cells compared to the survival of a control group (untreated cells as controls of 100% viability).

Cellular Uptake Studies

To determine the cellular uptake, KB cells were seeded at a density of 2×10^4 cells/well in 24-well plates and incubated for 36 h until 70% confluence reached. The medium was replaced by 500 μl medium containing different types of doxorubicin liposomes (PEG-LP-DOX, FA-LP-DOX, PEG/TAT-LP-DOX or FA/TAT-LP-DOX) at the concentration of 3 μg/ml for 1 h. The solution was removed, and the cells were washed with cold PBS. Nuclei were stained with Hoechst 33342 for 15 min, washed three times with PBS and finally cells were examined on fluorescent microscope (IX51, Olympus, Japan).

For quantitative analysis of the cellular uptake, KB cells were seeded at a density of 2×10^5 cells/well in 6-well plates, incubated for 48 h. Then cells were incubated with different types of doxorubicin liposomes (PEG-LP-DOX, FA-LP-DOX, PEG/TAT-LP-DOX or FA/TAT-LP-DOX) at the DOX concentration of 6 μg/ml for 1 h. After that, the cells were washed three times with PBS, detached with 0.25% trypsin, centrifuged at 1,000 rpm for 5 min and suspended in 0.5 ml of PBS. Then the cells were analyzed using a flow cytometry (FACSCalibur, BD Biosciences, USA) at FL2-channal. For each sample, 10,000 events were collected and KB cells cultured under normal conditions were served as the control. In the competition experiments, 500 μg/ml of free folate (FA) or 800 μg/ml of polylysine (PLL) was added to the cells 30 min prior to the addition of FA/TAT-LP-DOX (DOX concentration, 6 μg/ml). After 1 h incubation, the cells were analyzed quantitatively as described above. For the determination of uptake rate, cells were treated with PEG-LP-DOX, FA-LP-DOX or FA/TAT-LP-DOX at different time points (0.5, 1, 1.5, 2 and 3 h) at the DOX concentration of 6 μg/ml. Then the cells were analyzed quantitatively as described above.

Subcellular Localization of the Liposomes by Confocal Microscopy

A confocal laser scanning microscopy (CLSM, TCS-SP2, Leica, Germany) was used to investigate intracellular distribution of different types of doxorubicin liposomes. KB cells were seeded on coverslips (22×22 mm), cultured for 36 h at 37°C, and then incubated with FA-LP-DOX or FA/TAT-LP-DOX in DMEM medium respectively for 1 or 2 h at the DOX concentration of 6 μg/ml. After that, cells were incubated with 50 nM LysoTracker Green (60 min) and 10 mM Hoechst 33342 (15 min) to visualize lysosomes and nuclei, respectively, and then fixed in 4% paraformaldehyde. Finally the cells were washed three times with cold PBS, and observed with the laser scanning confocal microscope.

Investigation of the Mechanism Involved in the Uptake of FA/TAT-LP-DOX

To study the uptake pathways of FA-LP-DOX, TAT-LP-DOX and FA/TAT-LP-DOX, cells were treated with following inhibitors individually at chosen concentrations: 10 μg/ml of chlorpromazine, 40 μg/ml of colchicine or 40 μg/ml of filipin (30,31). The MTT assay was employed to confirm their toxicity. Cells cultured in presence of test liposomes but without inhibitors were used as controls and their fluorescence intensities were expressed as 100%. Following pre-incubation for 30 min, cells were treated with FA-LP-DOX, TAT-LP-DOX or FA/TAT-LP-DOX for 1 h, respectively. Then cells were washed three times with PBS and the fluorescence intensity of DOX was determined by flow cytometry. The subcellular distribution of FA/TAT-LP-DOX was also observed by confocal microscope after 30 min incubation with different endocytosis inhibitors and subsequent incubation with FA/TAT-LP-DOX for 2 h.

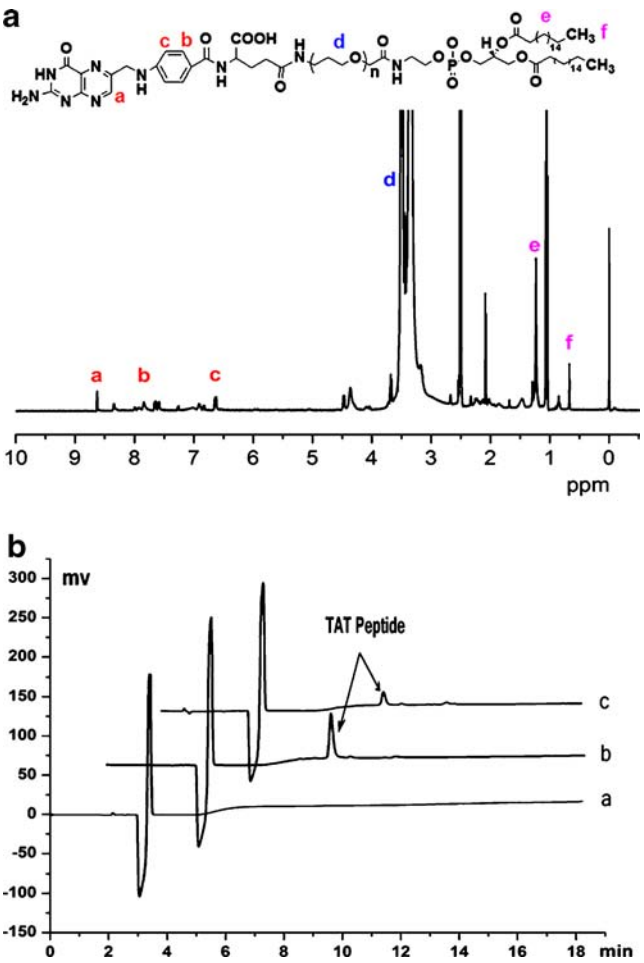

Fig. 2 Characterization of ligand-PEG-lipid conjugates. (**a**) The ^{1}H-NMR spectrum of DSPE-PEG$_{5000}$-FA. (**b**) HPLC assessment of TAT peptide conjugated to the distal end of DSPE-PEG$_{2000}$-Mal by monitoring absorbance at 220 nm. (*a* DSPE-PEG-Mal, *b* TAT peptide before reaction, *c* TAT peptide after reaction)

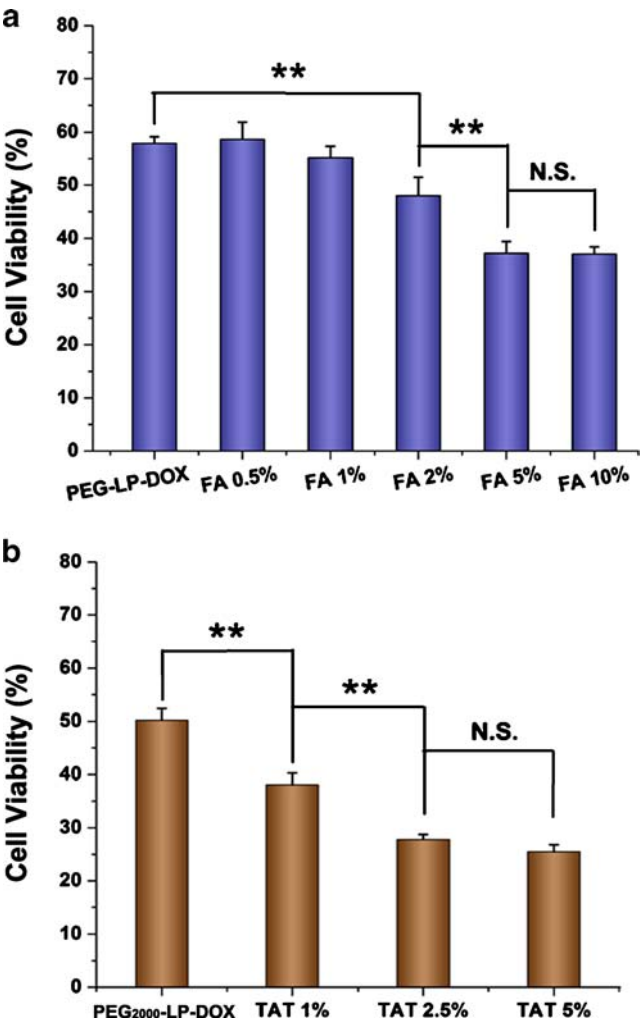

Fig. 3 *In vitro* cytotoxicity of FA-LP-DOX (**a**) or TAT-LP-DOX (**b**) with different density (molar ratio of ligands to lipid) of DSPE-PEG$_{5000}$-FA or DSPE-PEG$_{2000}$-TAT at 1.5μg/ml of DOX. Data are presented as means ± SD ($n = 3$). *$P < 0.05$, **$P < 0.01$, *N.S.* not significant.

In Vivo Imaging Investigations

Tumor-bearing mice were established as described previously. Briefly, about 1×10^7 KB cells were subcutaneously injected in the left flank of the mice. Tumors were allowed to grow to an average size of about 6 mm in diameter before the experiment. To investigate the tumor targeting efficacy of different types of liposomes *in vivo*, Cy7-labeled PEG/TAT-LP, FA-LP or FA/TAT-LP were injected into the tumor-bearing mice *via* tail vein at a dose of Cy7 0.4 mg/kg, respectively. At 6, 12, 18, 24, and 48 h post injection, the mice were anesthetized, and the whole body fluorescence images were acquired using a near-infrared fluorescence imaging system (Kodak, Rochester, New York) with a wavelength set at Ex = 747 nm, Em = 774 nm. During the imaging acquiring process, 3% isoflurane anesthesia was delivered *via* a nose cone system. The mean fluorescence intensity of Cy7-labeled liposomes in tumor region was calculated using the region of interest (ROI) function. Major organs and tumors were removed from the tumor-bearing mice at 48 h and finally visualized as described above.

Statistical Analysis

Comparisons between multiple treatments were made using one-way analysis of variance (ANOVA). Pair-wise comparisons between treatments were made using a student's *t*-test. $P < 0.05$ was considered significant.

RESULTS AND DISCUSSION

Synthesis of DSPE-PEG$_{5000}$-FA and DSPE-PEG$_{2000}$-TAT

The chemical structure of DSPE-PEG$_{5000}$-FA was confirmed by ^{1}H NMR spectrum (Fig. 2a), DSPE: 0.88 (t), 1.25 (s), PEG:

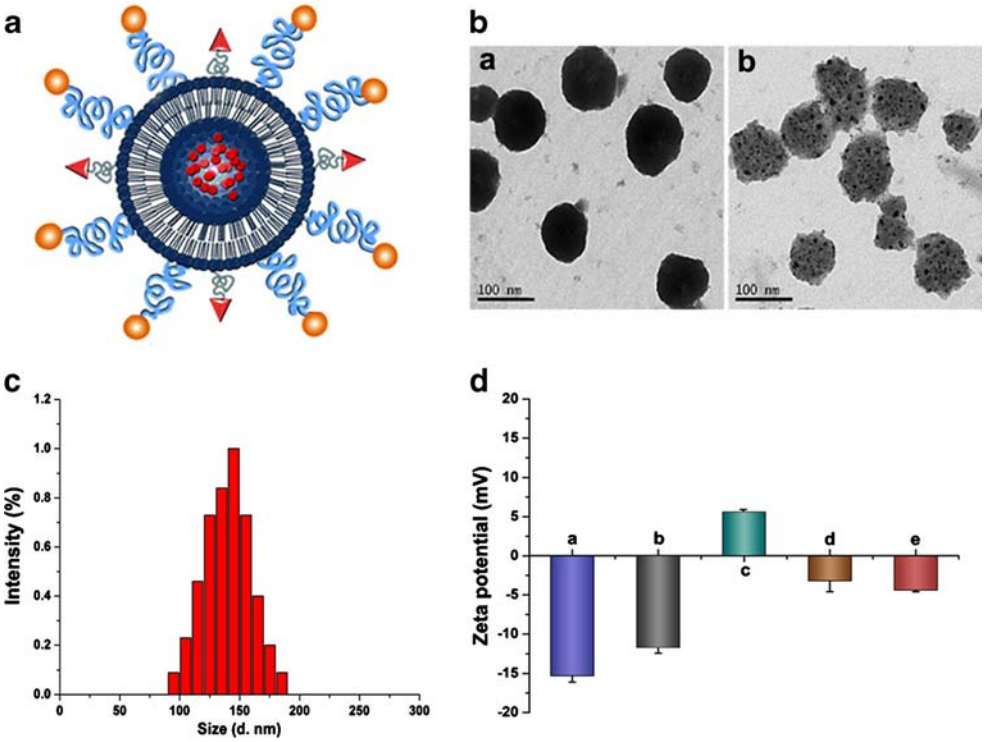

Fig. 4 Characterization of dual-ligand modified doxorubicin liposomes. (**a**) Schematic illustration of FA/TAT-LP-DOX. (**b**) TEM micrographs of LP-DOX (*a*) and FA/TAT-LP-DOX (*b*). (**c**) Particle size distribution of FA/TAT-LP-DOX. (**d**) Zeta potential of PEG-LP-DOX (*a*), FA-LP-DOX (*b*), TAT-LP-DOX (*c*), PEG/TAT-LP-DOX (*d*) and FA/TAT-LP-DOX (*e*).

3.50 (s), FA: 6.80 (d), 7.80 (t), 8.71 (s). The purity of DSPE-PEG_{5000}-FA was 85%, which was calculated by the integral area ratio. For DSPE-PEG_{2000}-TAT, TLC confirmed the formation of DSPE-PEG_{2000}-TAT as the spot of DSPE-PEG_{2000}-Mal disappeared after the reaction (data not shown). HPLC analysis was applied to determine the conjugation efficiency of TAT peptide to DSPE-PEG_{2000}-Mal. The retention time of TAT peptide was about 7.6 min, while NHS-PEG-Mal did not show obvious characteristic absorption peak under this condition (Fig. 2b, curve a). The conjugation efficiency was about 95% in accordance with the integrated areas of TAT peptide before and after reaction (Fig. 2b, curve b and c).

In Vitro Screening of the Optimal Ligand Density

For targeted nano drug delivery systems, the density of surface ligand is a key determinant for targeting efficiency (32). Low ligand density of nanoparticles makes it hard to satisfy specific recognition by cells, while high ligand density is prone to result in greater accumulation of nanoparticles in liver and spleen (4). Additionally, transmembrane ability of TAT peptide modified nanocarrier is believed to be tightly related to TAT peptide density (14,18). Therefore, prior to the construction of the dual-ligand liposome, a series of single-ligand liposomes with different ligand densities were firstly prepared and antitumor activities of these liposomes were examined by cytotoxicity assay. Figure 3a showed the relationship between FA density and cell viability. It was obvious that cell viability of

Table I Sizes, Zeta Potential and Entrapment Efficiency of Different Types of Liposomes ($n = 3$)

Type of liposomes	Particle size (nm)	Zeta potential (mV)	EE (%)
PEG-LP-DOX	145.6 ± 1.4	−15.3 ± 0.8	94.3 ± 1.3
FA-LP-DOX	148.2 ± 2.5	−11.7 ± 0.7	92.8 ± 2.3
TAT-LP-DOX	112.1 ± 2.3	5.6 ± 0.3	94.5 ± 1.8
PEG/TAT-LP-DOX	140.8 ± 3.4	−3.2 ± 1.4	93.2 ± 2.1
FA/TAT-LP-DOX	142.1 ± 1.2	−4.4 ± 0.2	92.2 ± 1.2

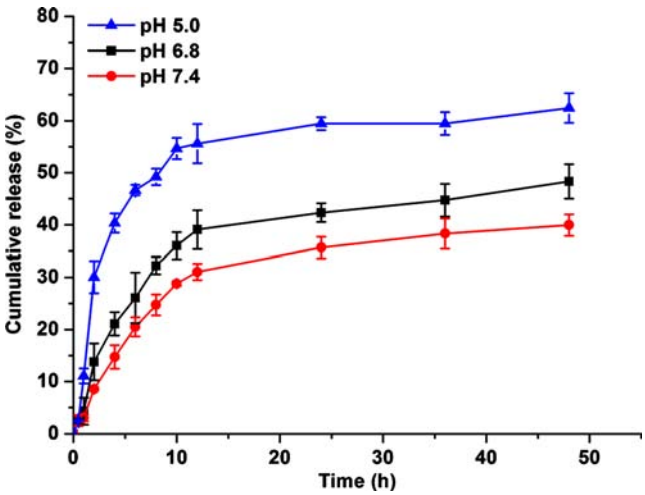

Fig. 5 *In vitro* release profiles of DOX from FA/TAT-LP-DOX at different pH values (pH 7.4, pH 6.8 and 5.0) at 37°C for 48 h. Data are expressed as the mean ± SD ($n = 3$).

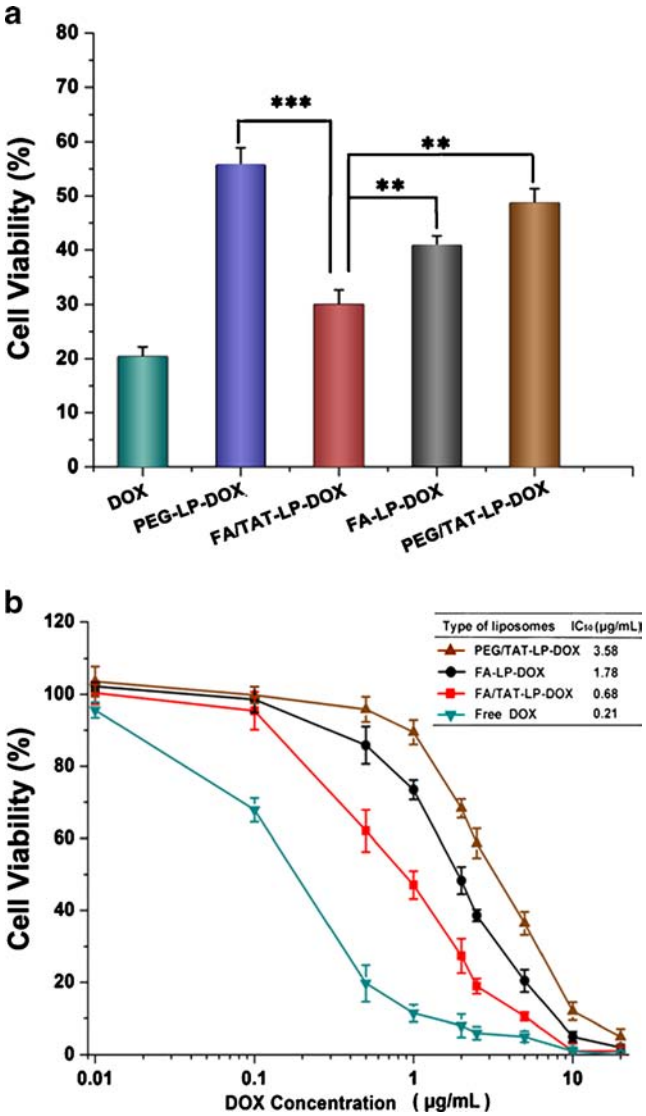

Fig. 6 (**a**) *In vitro* cytotoxicity of different types of liposomes at 1.5 μg/ml of DOX. (**b**) IC_{50} value of different types of liposomes from 0.01 to 20 μg/ml of DOX. Data are presented as means ± SD ($n=3$). *$P<0.05$, **$P<0.01$.

KB cells was gradually decreased with increased FA density. When FA density reached 5%, the lowest cell viability was obtained. However, no significant difference in cell viability was observed between 5% and 10% of FA density, suggesting that 5% of FA density was sufficient to occupy all the FA-receptors on cell surface. Similarly, cytotoxicity of TAT peptide modified liposome was highly dependent on TAT peptide density. Liposome with 5% of TAT peptide exhibited the strongest tumor killing activity (Fig. 3b). However, it was still noteworthy that no significant difference was found on cytotoxicity between liposomes with 2.5% and 5% of TAT peptide, indicating that 2.5% of TAT peptide was enough to exert transmembrane ability. Interestingly, it was found that with the equal drug loading and the same ligand density, TAT peptide modified liposomes always showed lower cell viability than FA modified liposomes, proving the advantage for TAT peptide in intracellular drug delivery.

Preparation and Characterization of the Dual-ligand Liposome

According to the above results, the dual-ligand liposome was constructed with 5% mol FA and 2.5% mol TAT peptide. For comparative analysis, liposomes with single-ligand modification or PEG modification only were also prepared. Physicochemical properties of these liposomes were shown in Fig. 4 and Table I. All the liposomes had a narrow size distribution, regular spherical shape and relatively high entrapment efficiency (above 90%). Interestingly, chain length of PEG seemed to affect the particle size of the liposomes. It was found that liposomes with long chain PEG, no matter with or without ligands, was about 30 nm larger in particle diameter than that of liposome with short chain PEG (about 110 nm for TAT-LP-DOX). The larger particles may provide a possible space to shield the TAT peptide. Data of zeta-potential determination further supported our assumption. The charge of TAT-LP-DOX was positive (5.6±0.3 mV), while the charge of either PEG-LP-DOX or FA-LP-DOX was negative, −15.3 ±0.8 mV and −11.7±0.7 mV, respectively. As for PEG/TAT-LP-DOX and FA/TAT-LP-DOX, pronounced changes in charge of the liposomes occurred. The determined zeta-potentials for PEG/TAT-LP-DOX and FA/TAT-LP-DOX were −3.2±1.4 mV and −4.4±0.2 mV, about 9 and 10 mV lower than that of TAT-LP-DOX. These findings suggested that cationic TAT peptide was able to be shielded by long chain PEG completely. In our case, slightly negative charge was considered necessary to repel opsonins, allowing the liposome to circulate in blood for a long time (33,34).

In Vitro Release of DOX

In vitro drug release of DOX from FA/TAT-LP-DOX was studied and this experiment was carried out at three different pH values (physiological pH 7.4, extracellular pH 6.8 and intracellular lysosomal pH 5.0). As shown in Fig. 5, a slow and sustained rather than burst release of DOX was observed at physiological pH 7.4, which is proposed for tumor targeted drug delivery, as during the blood circulation, the drug loss must be as less as possible to avoid its side effects. As the pH value of release medium decreased, the drug release became faster. At pH 5.0, nearly 60% of DOX was released after 48 h. This trend was consistent with the aforementioned drug-loading pH gradient method, and this pH-dependent phenomenon also benefited intracellular DOX release in the lysosomal acidic environment. Actually, the mechanisms for drug release from liposomes in lysosomes are complex, which involve pH-triggered release, membrane fusion triggered release, enzyme-triggered release and so on (35). Thus, the

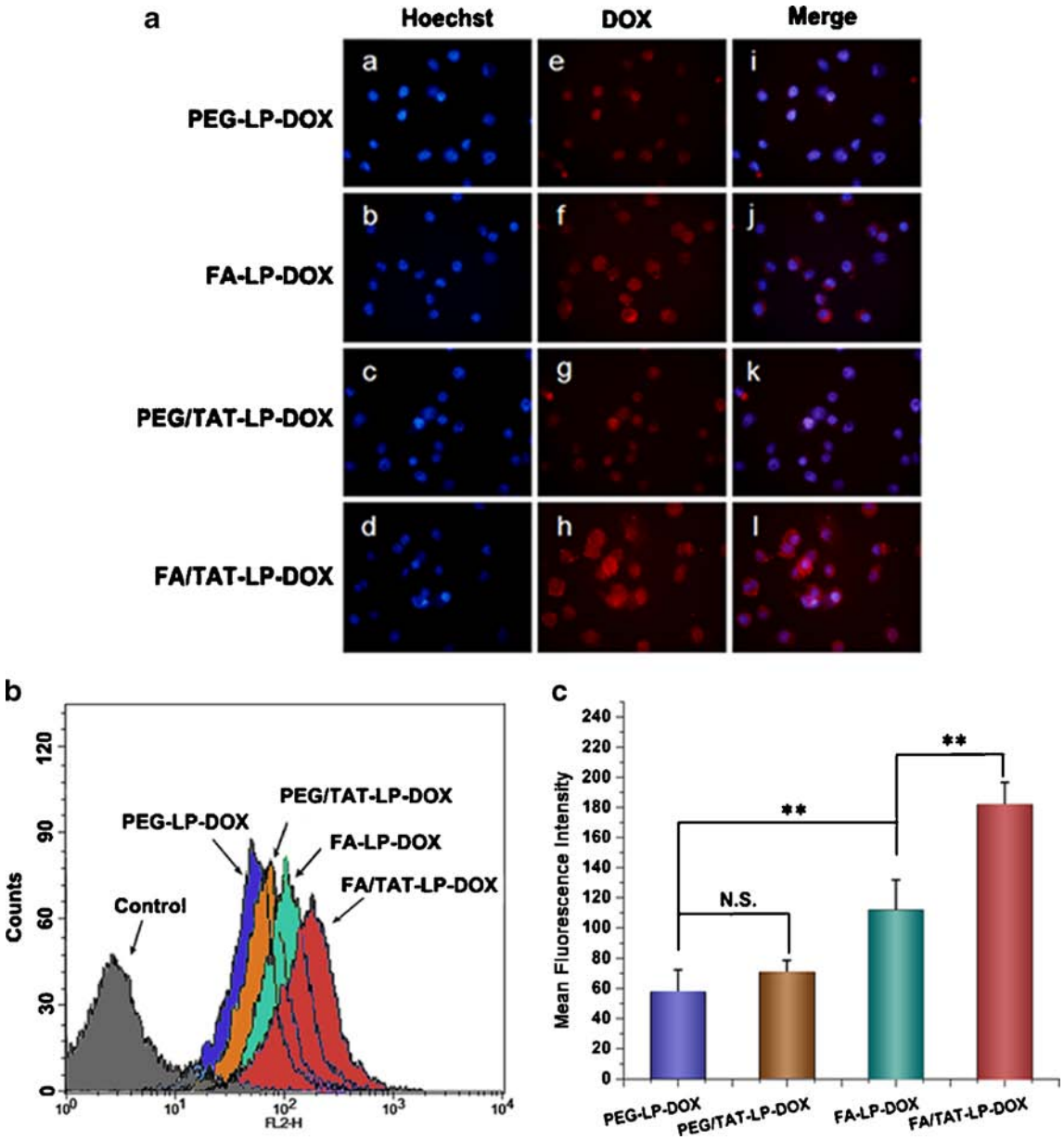

Fig. 7 Cellular uptake after 1 h culture with PEG-LP-DOX, FA-LP-DOX, PEG/TAT-LP-DOX or FA/TAT-LP-DOX. (**a**) Cellular uptake examined by fluorescent microscopy. *Blue*: Hoechst (*a–d*). *Red*: DOX (*e–h*). Merge: (*i–l*). (**b**) Flow cytometry analysis of different types of doxorubicin liposomes accumulated in KB cells. (**c**) Quantitation of mean fluorescent intensity of different types of doxorubicin liposomes by flow cytometry. Data are presented as means ± SD ($n = 3$). *$P < 0.05$, **$P < 0.01$, *N.S.* not significant.

in vitro drug release profiles only provided partial information on the intracellular DOX-release from FA/TAT-LP-DOX.

In Vitro Cytotoxicity Assay

Cytotoxicity assay was conducted to evaluate the antitumor activity of the dual-ligand liposomes. It could be seen in Fig. 6a that on the same experimental condition, FA/TAT-LP-DOX exhibited a significant decrease in cell viability compared with single-ligand liposomes FA-LP-DOX and PEG/TAT-LP-DOX ($P<0.01$). This result manifested the combination of FA and TAT peptide was beneficial to the antitumor efficacy of the liposome. Accidentally, cytotoxicity of PEG/TAT-LP-DOX was remarkably declined, which was approximate to that of PEG-LP-DOX, hinting that the translocation ability of TAT peptide was almost completely hindered by long chain PEG. IC_{50} (half maximal inhibitory concentration) determination offered further evidence for the greater antitumor efficacy of FA/TAT-LP-DOX. As displayed in Fig. 6b, the IC_{50} value of FA/TAT-LP-DOX (0.68 μg/ml) was 5.3-times and 2.6-times lower than that of PEG/TAT-LP-DOX (3.58 μg/ml) and FA-LP-DOX (1.78 μg/ml), respectively.

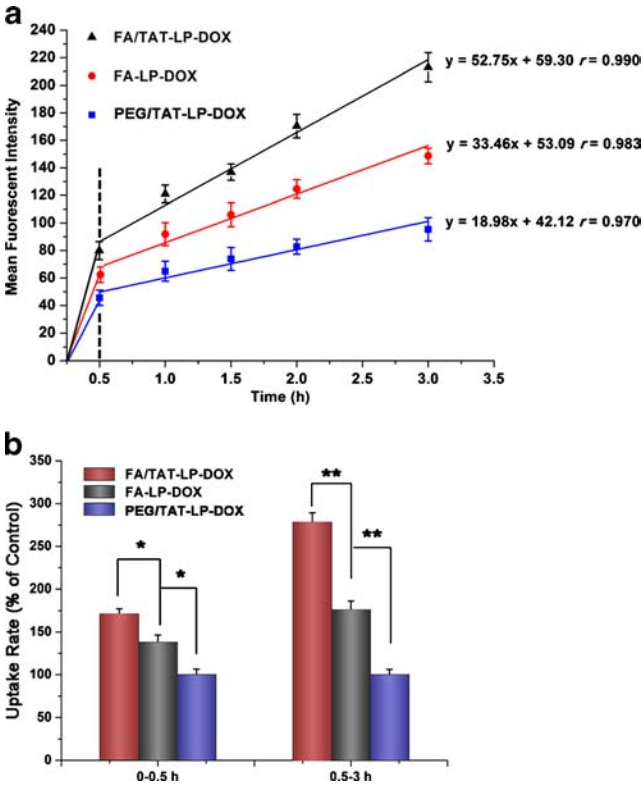

Fig. 8 (**a**) Linear fitting of the cellular uptake of KB cells incubated with different types of liposomes (FA/TAT-LP-DOX, FA-LP-DOX or PEG/TAT-LP-DOX) for various lengths of time (0.5, 1, 1.5, 2 and 3 h). (**b**) The relative uptake rate of different types of liposomes during 0–0.5 and 0.5–3 h. The uptake rate of PEG/TAT-LP-DOX was served as control (100%). Data are presented as means ± SD ($n = 3$). *$P < 0.05$, **$P < 0.01$.

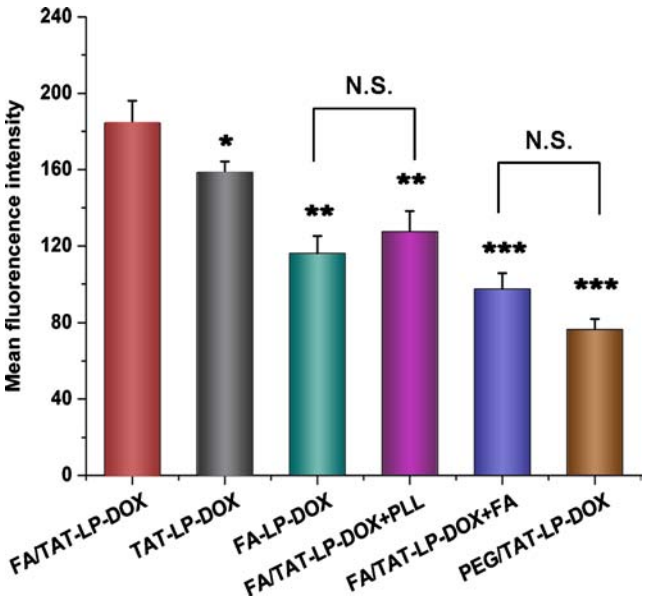

Fig. 9 Cellular uptake after 1 h culture with FA/TAT-LP-DOX, TAT-LP-DOX, FA-LP-DOX or PEG/TAT-LP-DOX examined by flow cytometry. In competition experiments, 500 μg/ml of free folate (FA) or 800 μg/ml of polylysine (PLL) was added to the cells 30 min prior to the addition of FA/TAT-LP-DOX. Data are presented as means ± SD ($n = 3$). *$P < 0.05$, **$P < 0.01$, ***$P < 0.001$ as compared with FA/TAT-LP-DOX. *N.S.* not significant.

Evaluations of Cellular Uptake

Cellular uptake of the liposomes was assessed by fluorescent microscopy. As shown in Fig. 7, after 1 h incubation, KB cells treated with FA-LP-DOX exhibited stronger red fluorescence in cytoplasm than those treated with PEG-LP-DOX, indicating decoration of FA could facilitate cellular uptake of the liposomes. As anticipated, fluorescence image for PEG/TAT-LP-DOX resembled that of PEG-LP-DOX. Together with the inferior tumor killing activity of PEG/TAT-LP-DOX, we could infer that long chain PEG in PEG/TAT-LP-DOX created a steric hindrance and blocked the association of TAT peptide with plasma membrane, leading to such an insufficient cellular uptake. As for FA/TAT-LP-DOX, the strongest red fluorescence was observed, suggesting that TAT peptide contributed to cellular uptake of FA/TAT-LP-DOX. Later, DOX fluorescence intensity in KB cells was analyzed by flow cytometry. FA/TAT-LP-DOX showed the highest mean fluorescence intensity, followed in a descending order by FA-LP-DOX > PEG/TAT-LP-DOX > PEG-LP-DOX (Fig. 7b and c). The mean fluorescence intensity of FA/TAT-LP-DOX was about 1.6-times and 2.6-times stronger than that of FA-LP-DOX and PEG/TAT-LP-DOX, respectively.

Further, uptake rates of FA-LP-DOX, PEG/TAT-LP-DOX and FA/TAT-LP-DOX by KB cells were investigated by determining the fluorescence intensities of DOX in cells at predetermined time points. As shown in Fig. 8a, the three types of liposomes presented distinct mean fluorescence intensities after 0.5 h incubation. The mean fluorescence intensity of FA/TAT-LP-DOX was about 1.2-times and 1.7-times stronger than that of FA-LP-DOX and PEG/TAT-LP-DOX, respectively. Later, differences in fluorescence intensity among the three types of liposomes were continuously widened as time prolonged. Interestingly, good linearity was observed between the mean fluorescence intensity and the incubation time by curve fitting using linear regression. In the time periods from 0.5 to 3 h, FA/TAT-LP-DOX had about 1.6-time and 2.8-time average uptake rate than that of FA-LP-DOX and PEG/TAT-LP-DOX, respectively (Fig. 8b). Thus, it was apparent that the combination of FA and TAT peptide not only remarkably boosted the liposomal uptake amount, but also significantly accelerated the liposomal uptake.

Competitive Inhibition Experiment

To explore the respective role of FA and TAT peptide in cellular uptake of the liposome, a competitive inhibition experiment was performed. Free FA and polylysine (PLL, positive charged) were used as the uptake inhibitors, which were expected to block folate receptor mediated endocytosis (22) and the electrostatic interaction between TAT peptide and

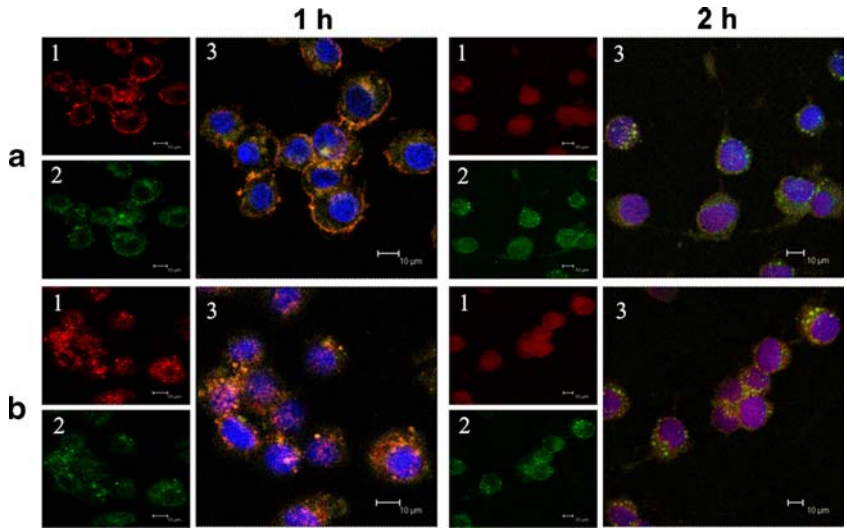

Fig. 10 Subcellular location of FA-LP-DOX (**a**) and FA/TAT-LP-DOX (**b**). Photos were taken after cells incubated with FA-LP-DOX or FA/TAT-LP-DOX for 1 or 2 h. Nuclei was stained by Hoechst 33342 (*blue*). *1*: red fluorescent DOX; *2*: green fluorescent late endosomes/lysosomes; *3*: overlay of 1, 2 and Nuclei. *Yellow*: Lysotracker Green co-localized with DOX. Bar: 10 μm.

plasma membrane (30), respectively. As shown in Fig. 9, cellular uptake of FA/TAT-LP-DOX was significantly suppressed after PLL or FA treatment. It was noteworthy that the determined fluorescence intensity of FA/TAT-LP-DOX treated by PLL was highly similar to that of FA-LP-DOX, indicating that inhibition of TAT peptide-mediated translocation did not affect FA receptor mediated endocytosis. Regarding to the case of treatment with FA, it was apparent that the determined mean fluorescence intensity of FA/TAT-LP-DOX was almost as close to that of PEG/TAT-LP-DOX and PEG-LP-DOX (not shown), but far less than that of TAT-LP-DOX. This result suggested that activation of translocation ability of TAT peptide relied heavily on the existence of specific ligand FA. It was probable that specific recognition and binding of FA to FA receptors on cell surface made TAT peptide fully exposed to plasma membrane, resulting in subsequent effective membrane penetration of TAT peptide (26).

Subcellular Localization of the Liposome by Confocal Microscope

Confocal laser scanning microscopy (CLSM) was used to observe intracellular trafficking of the liposomes. DOX-loaded liposomes were visualized as red fluorescence, lysosomes and nucleus were labeled with Lysotracker green (green fluorescence) and Hoechest 33342 (blue fluorescence), respectively. After 1 h incubation, FA-LP-DOX was observed primarily on the cytoplasmic side close to cell plasma membrane as shown by ring-shape red fluorescence (Fig. 10a), while FA/TAT-LP-DOX exhibited a uniform distribution of red fluorescence in the whole cytoplasm (Fig. 10b). In addition, strong yellow fluorescence in the cytoplasm derived from the overlapping of red fluorescence and green fluorescence was obvious for FA-LP-DOX and FA/TAT-LP-DOX treatment group, manifesting that both liposomes were transported into lysosomes after endocytosis. Further, it was clear that except for the yellow fluorescence in the cytoplasm, there was hardly any purple fluorescence visible in the nucleus for both liposomes at 1 h. This phenomenon pointed out that uptake of the liposomes was the predominant cellular activity instead of drug release in this time period. With the prolongation of time, a distinct situation was witnessed for both liposomes. Previous yellow fluorescence in the cytoplasm nearly disappeared, and was replaced by obvious green fluorescence. Meanwhile, strong purple fluorescence emerged in the nucleus. This change implied that the majority of DOX entrapped in the liposomes were librated and then entered the nucleus. Noticeably, the purple fluorescence for FA/TAT-LP-DOX was much stronger than that for FA-LP-DOX, reflecting that more DOX molecules entered the nucleus for FA/TAT-LP-DOX. It has been known that DOX exerts its cytotoxicity by chelating into the DNA, more DOX in the nucleus represents higher antitumor effect, according with the results of cytotoxcity assay. Additionally, it was worth mentioning that both liposomes showed similar intracellular transport behavior, but the fluorescence intensities observed in the nucleus were markedly different, indicating that uptake efficiency of liposome determined the drug amount delivered into the nucleus.

Uptake Mechanisms of the Dual-ligand Liposome

Nanocarriers can employ multiple pathways for cellular entry, mainly including clathrin-mediated endocytosis (CME), caveolae-mediated endocytosis and macropinocytosis (36). To elucidate the uptake mechanisms of FA/TAT-LP-DOX, we investigated the effect of different representative endocytic inhibitors on cellular uptake of FA/TAT-LP-DOX, namely, chlorpromazine (an inhibitor of CME) (37), colchicine (an

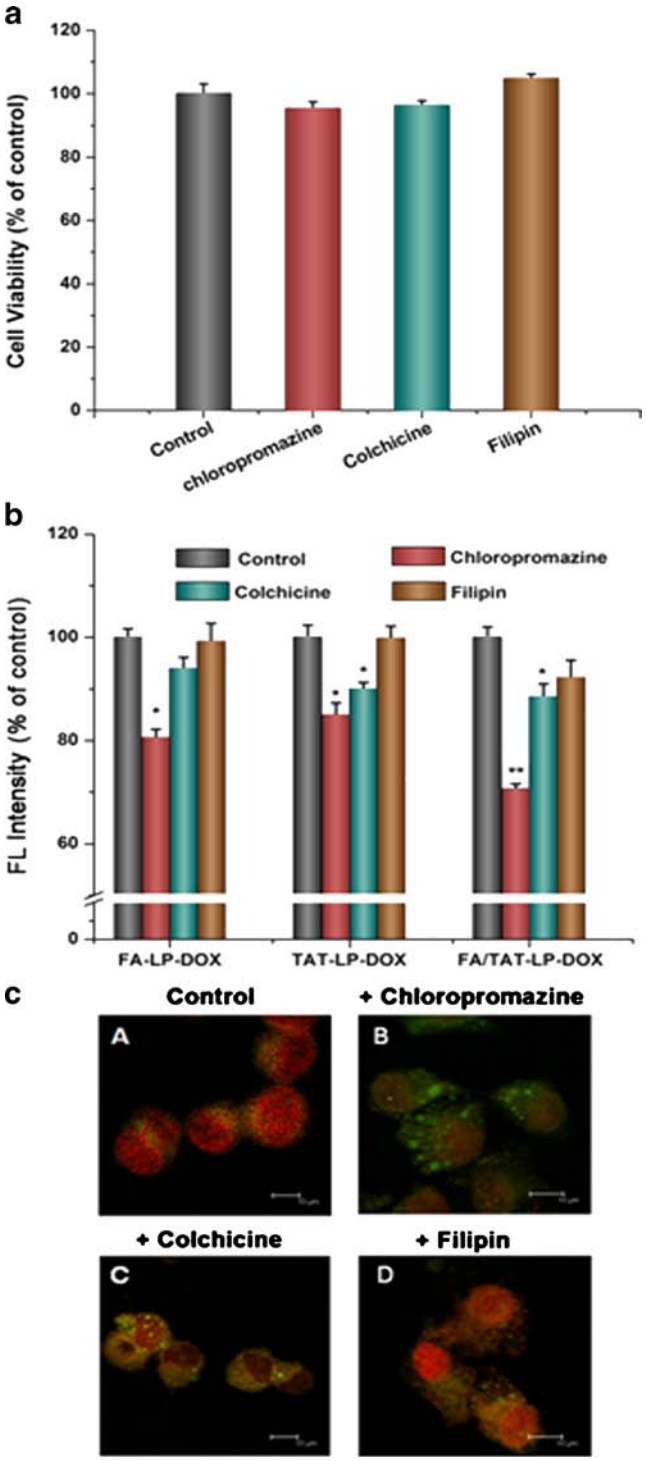

Fig. 11 (**a**) *In vitro* cytotoxicity of different endocytosis inhibitors. Cells cultured without inhibitors were served as control. (**b**) Percent inhibition of cellular uptake of FA-LP-DOX, TAT-LP-DOX and FA/TAT-LP-DOX in the presence of endocytosis inhibitors (chloropromazine, colchicine or filipin). Cells incubating with corresponding liposomes only were served as control. Data are presented as means ± SD ($n=3$). *$P<0.05$, **$P<0.01$. (**c**) Confocal laser scanning microscopy images of KB cells incubated with FA/TAT-LP-DOX for 2 h in the presence of chloropromazine (*b*), colchicine (*c*) or filipin (*d*). Cells incubating with FA/TAT-LP-DOX only were served as control (*a*). Bar: 10 μm.

inhibitor of macropinocytosis) (38) and filipin (an inhibitor of caveolae-mediated endocytosis) (31). Under the same condition, FA-LP-DOX and TAT-LP-DOX were served as the positive controls. Prior to the inhibition experiment, cytotoxicity of the three inhibitors at individual concentration was assessed and demonstrated nontoxic to the cells (Fig. 11a).

Figure 11b presented the results of cellular uptake of the three types of liposomes in the presence of different inhibitors. For FA-LP-DOX, only chlorpromazine among the three endocytic inhibitors significantly reduced the cellular uptake of FA-LP-DOX ($P<0.05$, 19.4%), indicating that CME was the major pathway for cellular entry of FA-LP-DOX. With regard to TAT peptide-mediated endocytosis, studies have suggested diversity of mechanisms for its translocation across the cellular membrane (18,39). Recent studies proposed that non-specific macropinocytosis was the main endocytic pathway for TAT-conjugated large molecules (40). In our case, it was revealed that both CME and macropinocytosis were the main endocytic routes for TAT-LP-DOX, as evidenced by 15.3% and 10.2% reduction in cellular uptake by chlorpromazine and colchicine treatment, respectively. As for FA/TAT-LP-DOX, even all known three endocytic pathways were involved into the cellular entry of these dual-ligand liposomes. Significantly, chlorpromazine and colchicine inhibited 29.2% and 11.5% of cellular uptake of the dual-ligand liposomes, respectively. Further, it was interesting to note that the inhibition rate of FA/TAT-LP-DOX by chlorpromazine approximated the summation of the corresponding inhibition rates of FA-LP-DOX and TAT-LP-DOX (34.7%), while the inhibition rate of FA/TAT-LP-DOX by colchicine was highly similar to that of TAT-LP-DOX (10.2%). This result suggested that it was very probable that FA and TAT peptide mediated the endocytosis of the dual-ligand liposome in their individual ways.

Further, confocal microscopy images directly showed the changes in cellular internalization of FA/TAT-LP-DOX after co-incubation with above inhibitors (Fig. 11c). Chlorpromazine almost completely blocked the clathrin-mediated endocytosis pathway, therefore apparent green fluorescence dots and absence of yellow fluorescence were observed in Fig. 11c-*b*. At the same time, severely weakened red fluorescence compared with the control was also seen in the nucleus, which could be ascribed to the liposomes internalized *via* the pathway of macropinocytosis-mediated endocytosis. In the case of colchicine (Fig. 11c-*c*), it presented a little inhibitory effect on FA/TAT-LP-DOX, as shown by somewhat diminished red fluorescence in the nucleus. This image agreed well with the data determined by flow cytometry (10.2% reduction in fluorescence intensity). As anticipated, filipin had negligible impact on the uptake of FA/TAT-LP-DOX (Fig. 11c-*d*). These observations, from another point of view, demonstrated that clathrin- and macropinocytosis-mediated endocytosis were the primary pathways for cellular entry of FA/TAT-LP-DOX.

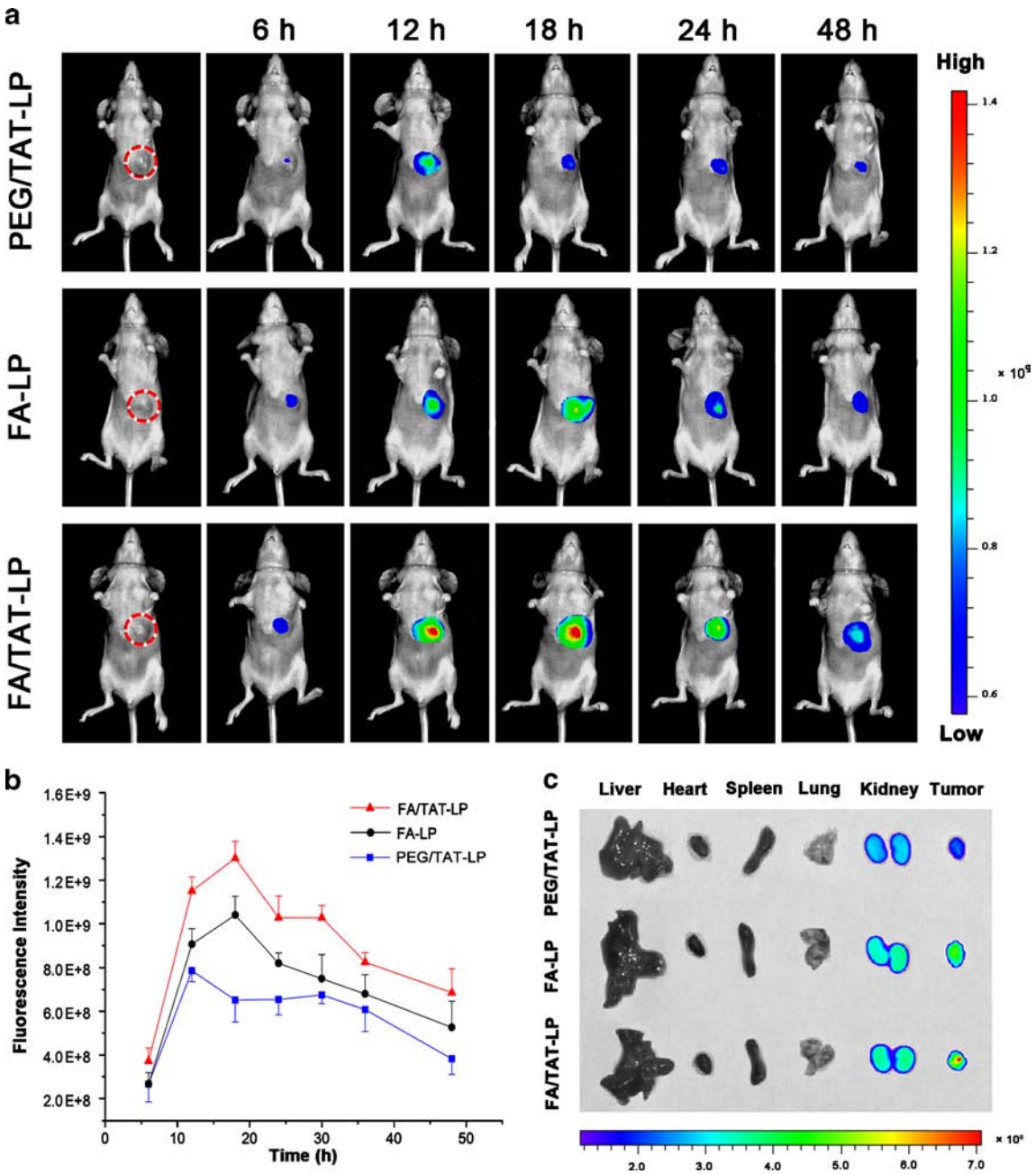

Fig. 12 The targeted delivery of PEG/TAT-LP, FA-LP or FA/TAT-LP to tumor-bearing mice *in vivo*. (**a**) Time-dependent *in vivo* fluorescent images of PEG-LP, FA-LP or FA/TAT-LP in KB tumor bearing mice. The *red dotted circles* indicate the sites of tumors. (**b**) Quantitative analysis of PEG/TAT-LP, FA-LP or FA/TAT-LP in tumor tissues estimated from the fluorescence intensities. Data are presented as means ± SD ($n = 3$). (**c**) *Ex vivo* images of organs and tumors at 48 h.

In Vivo **Targeted Delivery**

A noninvasive real-time imaging technique was used to monitor the dynamic distributions of Cy7-labeled PEG/TAT-LP, FA-LP and FA/TAT-LP in tumor bearing mice from 6 to 48 h post-injection. To avoid the interference of the strong fluorescence in liver, kidney and bladder as they are main metabolic and excretory organs, we applied the function of spectral unmixing only for tumor and its surrounding areas. The acquired fluorescence images and the corresponding fluorescence intensities of the Cy7-labeled liposomes in tumors were reflected in Fig. 12a and b, respectively. Clearly, all three types of liposomes showed tumor-selective accumulation, which could be explained by the EPR effect. However, it was noteworthy that PEG/TAT-LP always had the weaker fluorescence intensities in comparison with FA-LP and FA/TAT-LP, revealing that the transmembrane ability of TAT peptide was also effectively suppressed *in vivo* due to the

shielding of long chain PEG. Moreover, the fluorescence intensity of PEG/TAT-LP in tumors reached maximum value at 12 h post-injection, while the fluorescence intensities of FA-LP and FA/TAT-LP continuously increased until the maximum values were observed at 18 h. This time lag suggested that passive targeting was far from enough for nanocarriers to settle at tumor tissue and be taken by tumor cells. Interestingly, FA-LP and FA/TAT-LP exhibited similar profiles of fluorescence changes in intensity with time. But, we should be aware of the difference that stronger fluorescence intensities of FA/TAT-LP were attained at all the experimental time points. Obviously, this phenomenon could be ascribed to the synergistic effect of FA and TAT peptide on promoting fast uptake of FA/TAT-LP by tumor cells *in vivo*. As we know, rapid endocytosis of nanocarriers would create greater diffusion gradients which encouraged the directed transport of nanocarriers into tumor (4), thus substantially boosted the efficiency of tumor-targeted drug delivery. Specifically, resembling the *in vitro* experiments, it seemed that recognition and binding of FA to FA receptors triggered the cell-penetrating potential of TAT peptide *in vivo* in accordance with the inferior tumor accumulation of PEG/TAT-LP.

Figure 12c showed *ex vivo* images of main organs and tumors excised from the experimental animals at 48 h. It was evident that fluorescence signals only remained in kidney and tumors. Among them, FA/TAT-LP exhibited the strongest fluorescence signals in either kidney or tumor. These findings fully proved that the dual-ligand liposome was feasible to achieve long-term *in vivo* retention and superior tumor targeting.

CONCLUSIONS

In our work, liposomal nanocarriers with tumor-specific recognition and penetration properties were successfully constructed by a novel dual-ligand modification strategy. It was feasible to completely shield the positive charge of TAT peptide and hinder its translocation ability by introducing long chain PEG into the liposome, and we found that FA located on the outer surface of the liposome was essential for activating the translocation ability of TAT peptide. As demonstrated *in vitro*, the dual-ligand liposome exhibited stronger tumor killing activity and significantly improved cellular uptake efficiency compared with FA-LP-DOX and PEG/TAT-LP-DOX. In addition, uptake mechanism experiments revealed that FA and TAT peptide performed synergistically in promoting cellular uptake *via* clathrin- and macropinocytosis-mediated endocytosis. Importantly, the dual-ligand liposome retained cell-selective penetrating ability *in vivo*, and showed higher tumor accumulation than FA-LP. These studies demonstrated the superiority of FA/TAT-LP-DOX *in vitro* and *in vivo* and this dual-ligand modification strategy may provide an attractive approach for tumor-targeted intracellular drug delivery.

ACKNOWLEDGMENTS AND DISCLOSURES

We are grateful for the financial support from the Priority Academic Program Development of Jiangsu Higher Education Institutions (PAPD), National Natural Science Foundation of China (81173004, 81202473) and Natural Science Foundation of Jiangsu Province (BK2012182).

REFERENCES

1. Maeda H, Wu J, Sawa T, Matsumura Y, Hori K. Tumor vascular permeability and the EPR effect in macromolecular therapeutics: a review. J Control Release. 2000;65(1–2):271–84.
2. Iyer AK, Khaled G, Fang J, Maeda H. Exploiting the enhanced permeability and retention effect for tumor targeting. Drug Discov Today. 2006;11(17–18):812–8.
3. Danhier F, Feron O, Préat V. To exploit the tumor microenvironment: passive and active tumor targeting of nanocarriers for anticancer drug delivery. J Control Release. 2010;148(2):135–46.
4. Wang M, Thanou M. Targeting nanoparticles to cancer. Pharm Res. 2010;62(2):90–9.
5. Barenholz Y. Doxil®-the first FDA-approved nano-drug: lessons learned. J Control Release. 2012;160(2):117–34.
6. Li Y, Wang J, Wientjes MG, Au JLS. Delivery of nanomedicines to extracellular and intracellular compartments of a solid tumor. Adv Drug Deliv Rev. 2012;64(1):29–39.
7. Jang S, Wientjes MG, Lu D, Au JLS. Drug delivery and transport to solid tumors. Pharm Res. 2003;20(9):1337–50.
8. Jain RK. Transport of molecules across tumor vasculature. Cancer Metastasis Rev. 1987;6(4):559–93.
9. Gao Z, Zhang L, Sun Y. Nanotechnology applied to overcome tumor drug resistance. J Control Release. 2012;162(1):45–55.
10. James DB, Betancourt T, Brannon-Peppas L. Active targeting schemes for nanoparticle systems in cancer therapeutics. Adv Drug Deliv Rev. 2008;60(15):1615–26.
11. Thomas TP, Majoros IJ, Kotlyar A, Kukowska-Latallo JF, Bielinska A, Myc A, *et al.* Targeting and inhibition of cell growth by an engineered dendritic nanodevice. J Med Chem. 2005;48(11):3729–35.
12. Kunath K, Merdan T, Hegener O, Häberlein H, Kissel T. Integrin targeting using RGD-PEI conjugates for in vitro gene transfer. J Gene Med. 2003;5(7):588–99.
13. Levchenko TS, Rammohan R, Volodina N, Torchilin VP, Nejat D. Tat Peptide-mediated intracellular delivery of liposomes. In: Abelson JN, Simon MI, editors. Methods in enzymol. New York: Academic; 2003. p. 339–49.
14. Torchilin VP. Tat peptide-mediated intracellular delivery of pharmaceutical nanocarriers. Adv Drug Deliv Rev. 2008;60(4–5):548–58.
15. Fretz MM, Koning GA, Mastrobattista E, Jiskoot W, Storm G. OVCAR-3 cells internalize TAT-peptide modified liposomes by endocytosis. Biochim Biophys Acta (BBA) Biomembr. 2004;1665(1–2):48–56.
16. Vivès E. Cellular uptake of the Tat peptide: an endocytosis mechanism following ionic interactions. J Mol Recognit. 2003;16(5):265–71.

17. Drin G, Cottin S, Blanc E, Rees AR, Temsamani J. Studies on the internalization mechanism of cationic cell-penetrating peptides. J Biol Chem. 2003;278(33):31192–201.
18. Brooks H, Lebleu B, Vivès E. Tat peptide-mediated cellular delivery: back to basics. Adv Drug Deliv Rev. 2005;57(4):559–77.
19. Kuai R, Yuan W, Qin Y, Chen H, Tang J, Yuan M, *et al.* Efficient delivery of payload into tumor cells in a controlled manner by Tat and thiolytic cleavable PEG co-modified liposomes. Mol Pharm. 2010;7(5):1816–26.
20. Koren E, Apte A, Jani A, Torchilin VP. Multifunctional PEGylated 2C5-immunoliposomes containing pH-sensitive bonds and TAT peptide for enhanced tumor cell internalization and cytotoxicity. J Control Release. 2012;160(2):264–73.
21. Takara K, Hatakeyama H, Ohga N, Hida K, Harashima H. Design of a dual-ligand system using a specific ligand and cell penetrating peptide, resulting in a synergistic effect on selectivity and cellular uptake. Int J Pharm. 2010;396(1–2):143–8.
22. Saul JM, Annapragada A, Natarajan JV, Bellamkonda RV. Controlled targeting of liposomal doxorubicin via the folate receptor in vitro. J Control Release. 2003;92(1–2):49–67.
23. Lee RJ, Low PS. Folate-mediated tumor cell targeting of liposome-entrapped doxorubicin in vitro. Biochim Biophys Acta (BBA) Biomembr. 1995;1233(2):134–44.
24. Liu F, Park JY, Zhang Y, Conwell C, Liu Y, Bathula SR, *et al.* Targeted cancer therapy with novel high drug-loading nanocrystals. J Pharm Sci. 2010;99(8):3542–51.
25. Pan X, Wang H, Lee RJ. Antitumor activity of folate receptor-targeted liposomal doxorubicin in a KB oral carcinoma murine xenograft Model. Pharm Res. 2003;20(3):417–22.
26. Torchilin VP, Rammohan R, Weissig V, Levchenko TS. TAT peptide on the surface of liposomes affords their efficient intracellular delivery even at low temperature and in the presence of metabolic inhibitors. Proc Natl Acad Sci U S A. 2001;98(15):8786–91.
27. Nobs L, Buchegger F, Gurny R, Allémann E. Current methods for attaching targeting ligands to liposomes and nanoparticles. J Pharm Sci. 2004;93(8):1980–92.
28. Veronese FM, Pasut G. PEGylation, successful approach to drug delivery. Drug Discov Today. 2005;10(21):1451–8.
29. Wu J, Liu Q, Lee RJ. A folate receptor-targeted liposomal formulation for paclitaxel. Int J Pharm. 2006;316(1–2):148–53.
30. Zhu S, Hong M, Zhang L, Tang G, Jiang Y, Pei Y. PEGylated PAMAM dendrimer-doxorubicin conjugates: in vitro evaluation and in vivo tumor accumulation. Pharm Res. 2010;27(1):161–74.
31. Peng SF, Tseng MT, Ho YC, Wei MC, Liao ZX, Sung HW. Mechanisms of cellular uptake and intracellular trafficking with chitosan/DNA/poly(γ-glutamic acid) complexes as a gene delivery vector. Biomaterials. 2011;32(1):239–48.
32. Qhattal HSS, Liu X. Characterization of CD44-mediated cancer cell uptake and intracellular distribution of hyaluronan-grafted liposomes. Mol Pharm. 2011;8(4):1233–46.
33. Lee JS, Ankone M, Pieters E, Schiffelers RM, Hennink WE, Feijen J. Circulation kinetics and biodistribution of dual-labeled polymersomes with modulated surface charge in tumor-bearing mice: comparison with stealth liposomes. J Control Release. 2011;155(2):282–8.
34. Xiao K, Li Y, Luo J, Lee JS, Xiao W, Gonik AM, *et al.* The effect of surface charge on in vivo biodistribution of PEG-oligocholic acid based micellar nanoparticles. Biomaterials. 2011;32(13):3435–46.
35. Allen TM, Cullis PR. Liposomal drug delivery systems: from concept to clinical applications. Adv Drug Deliv Rev. 2013;65(1):36–48.
36. Sahay G, Alakhova DY, Kabanov AV. Endocytosis of nanomedicines. J Control Release. 2010;145(3):182–95.
37. Un K, Sakai-Kato K, Oshima Y, Kawanishi T, Okuda H. Intracellular trafficking mechanism, from intracellular uptake to extracellular efflux, for phospholipid/cholesterol liposomes. Biomaterials. 2012;33(32):8131–41.
38. Kitchens KM, Kolhatkar RB, Swaan PW, Ghandehari H. Endocytosis inhibitors prevent poly(amidoamine) dendrimer internalization and permeability across Caco-2 cells. Mol Pharm. 2008;5(2):364–9.
39. Vandenbroucke RE, De Smedt SC, Demeester J, Sanders NN. Cellular entry pathway and gene transfer capacity of TAT-modified lipoplexes. Biochim Biophys Acta (BBA) Biomembr. 2007;1768(3):571–9.
40. Ruan G, Agrawal A, Marcus AI, Nie S. Imaging and tracking of Tat peptide-conjugated quantum dots in living cells: new insights into nanoparticle uptake, intracellular transport, and vesicle shedding. J Am Chem Soc. 2007;129(47):14759–66.